Ensemble Kalman filter data assimilation for a process-based catchment scale model of surface and subsurface flow

Matteo Camporese,[1] Claudio Paniconi,[2] Mario Putti,[3] and Paolo Salandin[1]

Received 27 March 2008; revised 25 June 2009; accepted 27 July 2009; published 15 October 2009.

[1] A sequential data assimilation procedure based on the ensemble Kalman filter (EnKF) is introduced and tested for a process-based numerical model of coupled surface and subsurface flow. The model is based on the three-dimensional Richards equation for variably saturated porous media and a diffusion wave approximation for overland and channel flow. A one-dimensional soil column experiment and a three-dimensional tilted v-catchment test case are presented. A preliminary analysis of the assimilation scheme is undertaken for the one-dimensional test case in order to validate the implementation by comparison with published results and to assess the influence of various factors on the filter's performance. The numerical results suggest robustness with respect to the ensemble size and provide useful information for the more complex tilted v-catchment test case. The assimilation frequency and the effects induced by data assimilation on the surface and/or subsurface system states are then evaluated for the v-catchment experiment using synthetic observations of pressure head and streamflow. The results suggest that streamflow prediction can be improved by assimilation of pressure head and streamflow, either individually or in tandem, whereas assimilation of streamflow data alone does not improve the subsurface system state. In terms of the global system state, i.e., surface and subsurface variables, frequent updates are especially beneficial when assimilating both pressure head and streamflow. Furthermore, it is shown that better evaluation of the subsurface volume resulting from assimilation of head data is crucial for improving subsequent surface response.

Citation: Camporese, M., C. Paniconi, M. Putti, and P. Salandin (2009), Ensemble Kalman filter data assimilation for a process-based catchment scale model of surface and subsurface flow, *Water Resour. Res.*, *45*, W10421, doi:10.1029/2008WR007031.

1. Introduction

[2] Catchment dynamics is strongly influenced by subsurface processes. Recent experimental evidence [e.g., *Kosugi et al.*, 2008] shows that groundwater flow is responsible for most of the observed streamflow in a headwater catchment, while *Wörman et al.* [2007] and *Kollet and Maxwell* [2008a, 2008b] show the important contribution of subsurface processes to the formation of streamflow in large scale catchments. Thus the use of a model capable of simulating surface-subsurface water interactions is of paramount importance in fully capturing the dynamics of catchment hydrology. This has led to the development of several recent models for the distributed, process-based simulation of coupled surface and subsurface flow [e.g., *VanderKwaak and Sudicky*, 1999; *Morita and Yen*, 2002; *Panday and Huyakorn*, 2004; *Kollet and Maxwell*, 2006; *Camporese et al.*, 2009]. Models such as these allow a more accurate description of critical hydrological processes such as rainfall-runoff-infiltration partitioning, soil moisture redistribution, groundwater recharge, and stream-aquifer interactions. Nevertheless, uncertainties and inaccuracies in model structure, parameter estimates (including boundary conditions), and observation data induce errors in the model predictions. Data assimilation (DA), which allows the merging of information from spatially and temporally distributed observations and model simulations, is an effective technique to improve prediction accuracies and quantify uncertainties [*McLaughlin*, 2002].

[3] Although not as common as DA applications in climate and land surface modeling, several data assimilation schemes have been used in conjuction with process-based subsurface models. The classic Kalman filter (KF [*Kalman*, 1960]) yields the best unbiased estimate of the measurement update if the system dynamics is linear and the system noise is a multidimensional Gaussian process. As such, it is suitable for saturated groundwater flow problems and has been used for example to reduce uncertainty in parameter estimation [*Hantush and Mariño*, 1997]. For nonlinear dynamics, the extended Kalman filter (EKF) has been developed by linearizing the system equations along a reference state trajectory based on the previous state estimate. *Entekhabi et al.* [1994] demonstrated the potential of EKF to retrieve soil moisture and temperature profiles in a soil column for a one-dimensional model of coupled heat and moisture diffusion in porous media. In an application

[1] Dipartimento di Ingegneria Idraulica, Marittima, Ambientale e Geotecnica, Università degli Studi di Padova, Padova, Italy.
[2] Institut National de la Recherche Scientifique, Centre Eau, Terre et Environnement, Université du Québec, Quebec, Quebec, Canada.
[3] Dipartimento di Metodi e Modelli Matematici per le Scienze Applicate, Università degli Studi di Padova, Padova, Italy.

0043-1397/09/2008WR007031$09.00

based on the one-dimensional Richards equation, *Hoeben and Troch* [2000] found that EKF provides accurate retrieval of the moisture profile from sporadic measurements at the surface. Both KF and EKF require the covariance matrices expressing system noise statistics to be explicitly set, and their evaluation must be based on physical considerations. For groundwater modeling applications this important issue has been addressed for instance by *Van Geer et al.* [1991] and *Drécourt et al.* [2006].

[4] Due to computational and stability limitations [e.g., *Miller et al.*, 1994; *Reichle et al.*, 2002b], the Kalman and extended Kalman filters are impractical for detailed numerical models of surface-subsurface interactions, where a three-dimensional discretization is used for the subsurface and where flow across the land surface-atmosphere interface and within the soil (unsaturated) zone can be strongly nonlinear. DA studies based on such models have thus been limited to simpler schemes such as nudging [*Paniconi et al.*, 2003]. A more sophisticated scheme applicable to large scale nonlinear problems is the ensemble Kalman filter (EnKF), which uses an ensemble of model trajectories from which the necessary error covariances are estimated at the time of an update [*Evensen*, 1994]. Many studies have recently focused on various aspects of data assimilation for land surface modeling: the sensitivity of EnKF to ensemble size [*Reichle et al.*, 2002b]; an intercomparison between the EnKF and EKF [*Reichle et al.*, 2002a] and between one-dimensional and two-dimensional applications of the EnKF [*Reichle and Koster*, 2003]; the impact of observation frequency [*Walker and Houser*, 2001] and model bias [*De Lannoy et al.*, 2007]; and the potential benefit of assimilating streamflow [*Pauwels and De Lannoy*, 2006] and both soil moisture and streamflow [*Crow and Van Loon*, 2006]. To a more limited extent, EnKF has been used in simple subsurface models such as the one-dimensional Richards equation [*Das and Mohanty*, 2006], three-dimensional saturated groundwater flow [*Chen and Zhang*, 2006], and conceptual rainfall-runoff modeling [*Aubert et al.*, 2003; *Clark et al.*, 2008].

[5] Land surface models [e.g., *Chen et al.*, 1996; *Liang et al.*, 1996; *Koster and Suarez*, 1996; *Dai et al.*, 2003] typically include a thin surface soil layer coupled to one or several thicker root zone layers. They use simplified representations of lateral subsurface flow and neglect deeper groundwater flow. To improve the simulation of catchment dynamics, there is a need for robust assimilation of measurement information, both from remote sensing and local observations, into more complex, coupled surface-subsurface models [*Maxwell and Kollet*, 2008].

[6] In this study the ensemble Kalman filter is applied to a process-based catchment scale model of surface and subsurface flow. Following a brief presentation of the hydrological model, the EnKF implementation is described for a configuration in which both surface (e.g., ponding head, streamflow) and subsurface (e.g., pressure head, soil moisture) observations can be assimilated. The behavior and performance of the filter are then analyzed with reference to two synthetic test cases: (1) a one-dimensional soil column retrieval experiment, where comparisons are made with the EKF results of *Walker et al.* [2001] and where the numerical sensitivity with respect to various factors (e.g., ensemble size, noise statistics) is assessed; and (2) a three-dimensional v-shaped catchment rainfall-drainage experiment, where, for different assimilation frequencies and different scenarios of state variable observations (streamflow only, pressure head only, both), the model is evaluated in terms of its ability to retrieve the correct watershed response.

2. Methods

2.1. Model Description

[7] The CATHY (CATchment HYdrology) model simulates subsurface, overland, and channel flow by integrating the three-dimensional Richards equation for variably saturated porous media with a one-dimensional diffusion wave approximation of the de Saint Venant equation for surface water dynamics [*Bixio et al.*, 2000; *Camporese et al.*, 2009]:

$$S_w S_s \frac{\partial \psi}{\partial t} + \phi \frac{\partial S_w}{\partial t} = \nabla \cdot [K_s K_r(S_w)(\nabla \psi + \eta_z)] + q_s(h), \qquad (1)$$

$$\frac{\partial Q}{\partial t} + c_k \frac{\partial Q}{\partial s} = D_h \frac{\partial^2 Q}{\partial s^2} + c_k q_L(h, \psi), \qquad (2)$$

where $S_w = \theta/\phi$ is water saturation, θ is the volumetric soil moisture content [/], ϕ is the porosity or saturated moisture content, S_s is the aquifer specific storage coefficient [L^{-1}], ψ is pressure head [L], t is time [T], ∇ is the gradient operator, K_s is the saturated hydraulic conductivity tensor [L/T], K_r is the relative hydraulic conductivity function [/], $\eta_z = (0, 0, 1)^T$, z is the vertical coordinate directed upward [L], and q_s represents distributed source (positive) or sink (negative) terms [L^3/L^3T]. The surface water is routed using equation (2) along each single hillslope or channel link using a one-dimensional coordinate system s [L] defined on the drainage network. In this equation, Q is the discharge along the channel link [L^3/T], c_k is the kinematic wave celerity [L/T], D_h is the hydraulic diffusivity [L^2/T], and q_L is the inflow (positive) or outflow (negative) rate from the subsurface to the surface [L^3/LT]. The fluxes q_s and q_L are both functions of ponding head h [L], which is obtained from the discharge Q via a mass balance calculation. The soil hydraulic properties are specified by K_s and by families of characteristic (constitutive) relationships $S_w(\psi)$ and $K_r(\psi)$ [e.g., *van Genuchten*, 1980]. Some features of the model relevant to the EnKF implementation and simulation examples are briefly described here.

[8] The strong nonlinearities in the model arise from the unsaturated soil hydraulic functions and from the dependence of q_s and q_L on ponding head. Spatial discretization proceeds from a digital elevation model (DEM) representing the catchment surface. These DEM cells are triangulated and replicated vertically to form a three-dimensional tetrahedral grid for the underlying soil and aquifer. Precipitation fluxes during storm events and potential evaporation during interstorm periods are the main driving forces of the model. The catchment partitions this atmospheric forcing into surface runoff, infiltration, actual evaporation, and changes in storage via a surface boundary condition switching algorithm [*Putti and Paniconi*, 2004]. Surface saturation or ponding can occur via the infiltration excess or saturation excess mechanisms, and both of these are automatically accounted for by the same switching algorithm. Overland

flow is assumed to concentrate in rills or rivulets confined to "hillslope" cells (upstream drainage area A [L^2] below some prescribed threshold A^*), while channel flow occurs on "stream" cells ($A \geq A^*$) [*Montgomery and Foufoula-Georgiou*, 1993]. Retardation and storage effects due to lakes or topographic depressions are implemented via a lake boundary-following procedure [*Mackay and Band*, 1998]. The subsurface equation (1) is solved by the finite element method [*Paniconi and Putti*, 1994], whereas an explicit time discretization based on the Muskingum-Cunge scheme is used for the overland flow equation (2) [*Orlandini and Rosso*, 1996].

2.2. Implementation of EnKF for the Coupled Model

[9] The ensemble Kalman filter uses a Monte Carlo technique to approximate the probabilistic information conveyed by the conditional probability density functions (PDFs) of the system state given the measurements. This is done by generating an ensemble of model predictions from which the error/covariance information, used in the Kalman filter to update model predictions with observations, is estimated [*Evensen*, 1994]. This avoids the need to explicitly propagate the covariance matrix, an advantage over other KF-based methods such as the extended Kalman filter. For our three-dimensional nonlinear numerical model, the Jacobian calculations needed to explicitly derive the covariance matrix at each step of a simulation would be computationally prohibitive. In EnKF by contrast, the size of the ensemble may be quite small relative to the size of the variable space, especially for large problems. Other attractive characteristics of EnKF for our application are that its implementation does not require the linearization of the model, its sequential structure is convenient for processing periodic measurements (e.g., soil moisture from satellite sensors, groundwater levels from well loggers) in real time, it provides information on the accuracy of its estimates, and it is able to account for a wide range of possible model errors [*Reichle et al.*, 2002b]. On the other hand, EnKF requires a large amount of memory to construct, store, and manipulate large covariance matrices, and, though not as costly as EKF, it is still quite computationally demanding for large numerical grids.

[10] In our implementation the system state is expressed in terms of pressure head ψ for each node of the three-dimensional subsurface grid and in terms of streamflow (both inflow Q^{in} and outflow Q^{out}) for each cell of the surface DEM discretization. The formulation includes both inflow and outflow discharges because in the Muskingum-Cunge scheme the outflow discharge for each cell is computed by the following expression:

$$Q_{i+1}^{k+1} = C_1 Q_i^{k+1} + C_2 Q_i^k + C_3 Q_{i+1}^k + C_4 q_{s_{i+1}}^k,$$

where Q_{i+1}^{k+1} is outflow discharge at network point $(i + 1)\Delta s$ and time $(k + 1)\Delta t$, which depends not only on the discharge at the same network point and previous time Q_{i+1}^k, but also on the outflow discharge at the upstream network point (i.e., inflow at the current network point) at the present (Q_i^{k+1}) and previous (Q_i^k) times. The cell inflow and outflow fluxes are allocated in different vectors and their difference is used in a mass balance calculation that evaluates the exchange flux q_s with the subsurface [*Camporese et al.*, 2009]. Thus at the time of an update we reinitialize both inflow and outflow fluxes.

[11] We consider a number NMC of state vectors consisting of the pressure heads and inflow and outflow fluxes:

$$y^j(t) = \left\{ \psi_1 \dots \psi_N, Q_1^{in} \dots Q_{N_{CEL}}^{in}, Q_1^{out} \dots Q_{N_{CEL}}^{out} \right\}^j, \quad j = 1, \dots, NMC, \tag{3}$$

where NMC is the ensemble size (number of realizations) and the state vector y^j has dimension $N_y = N + N_{CEL} + N_{CEL}$, with N the number of nodes of the three-dimensional grid and N_{CEL} the number of surface cells. The basic goal of the data assimilation procedure is to estimate these uncertain states by combining information from a physical model and from available hydrological measurements. The observation data considered in this study are a mix of soil moisture, pressure head, and streamflow measurements. In theory any combination of surface and subsurface observations can be accommodated in the implementation presented here.

[12] Each uncertain state vector is propagated in time by the CATHY model with uncertain inputs. The model, based on the mass and momentum conservation principles expressed in equations (1) and (2), can be written concisely as a vector-valued discrete-time state equation:

$$y^j(t) = A\left[y^j(\tau), \beta^j, u^j\ (t), t, \tau\right];\ t_0 \leq \tau < t;\ y^j(t_0) = y_0^j, \tag{4}$$

with j = 1,. . ., NMC. The vectors β^j represent the time-invariant sets of soil parameters (saturated hydraulic conductivity, specific storage, porosity, retention curve parameters, etc.) while the vectors $u^j(t)$ represent the time-dependent atmospheric forcing variables (precipitation or evaporation). The initial condition at time $t = t_0$ is given by y_0^j and the nonlinear operator A describes how the state at a previous time τ is related to the state at time t. Inputs (soil parameters and atmospheric forcings) and states are all treated as random variables in order to account for uncertainties in their values. The statistical properties of the random inputs are discussed in the following section.

[13] In order to estimate the system states from hydrological measurements, it is necessary to define a transfer model M that describes how observed variables are related to the system states. As for the state equation, this model can be concisely expressed as a vector-valued discrete-time measurement equation:

$$z_i^j = M\left[y^j, \omega_i^j, t_i\right], \tag{5}$$

where z_i^j is the j^{th} of NMC vectors containing pressure head and/or soil moisture and/or streamflow data obtained at time t_i and ω_i^j is a random noise term that accounts for measurement errors. The statistical properties of the random noise term are assumed known, as discussed in the next section.

[14] At time t_0, the state vector $y^j(t)$ associated with replicate j is initialized with a randomly perturbed realization of the known initial condition y_0. Analogously, each time-invariant vector β^j is generated by randomly perturbing the known set of soil parameters β. For each replicate,

the state vector is propagated forward in time to the first measurement time t_1, according to equation (4). Randomly perturbed values $u^j(t)$ of the known atmospheric inputs $u(t)$ are inserted into equation (4) at each simulation time step. At t_1 each replicate is updated (or conditioned) to reflect the effect of the measurement z_1. The updated states become the initial conditions for the next time period (t_1, t_2]. This process continues sequentially: first a propagation step over each interval between measurement times t_i and t_{i+1} and then an update step at each measurement time t_{i+1}. This two-step structure is characteristic of Kalman filter methods.

[15] The update step is expressed as [*Margulis et al.*, 2002]:

$$y^j(t_{i+1}|Z_{i+1}) = y^j(t_{i+1}|Z_i) + K_{i+1}\left\{z^j_{i+1} - M\left[y^j(t_{i+1}|Z_i)\right]\right\}, \quad (6)$$

where the Kalman gain K_{i+1} is a measure of the relative level of confidence given to the model and to the measurements. The updated states are written $y^j(t_{i+1}|Z_{i+1})$ to indicate their dependence on all measurements collected through t_{i+1}. The Kalman gain is dependent on the system state covariance matrix C_{yy} and the measurement error covariance matrix $C_{\omega\omega}$, both determined by sampling the ensemble statistics, even though C_{yy} is never explicitly computed. Denoting by $Y(t_{i+1}|Z_i)$ the matrix whose columns are the NMC state vectors $y^j(t_{i+1}|Z_i)$, we can define the matrix $Y'(t_{i+1}|Z_i)$ as the deviation from the ensemble average:

$$Y'(t_{i+1}|Z_i) = Y(t_{i+1}|Z_i) - \overline{Y}(t_{i+1}|Z_i).$$

The Kalman gain can thus be expressed as:

$$K_{i+1} = Y'(t_{i+1}|Z_i)Y'^T(t_{i+1}|Z_i)H^T \cdot \left[HY'(t_{i+1}|Z_i)Y'^T(t_{i+1}|Z_i)H^T + C_{\omega\omega}\right]^{-1}, \quad (7)$$

where the matrix H represents the linearization of the measurement operator M.

[16] The transfer model M is linear when pressure head and streamflow data are assimilated, and in this case $H = M$ is simply a matrix of 1s and 0s. In the case of soil moisture assimilation (or other observation variables that are nonlinearly related to the state variables), different methods are available for linearizing the operator M. For instance, the matrix H can be computed numerically as the first derivative of the soil moisture with respect to the pressure head [*Reichle et al.*, 2002b].

[17] Alternatively, an approximate treatment of M known as the state augmentation technique [*Evensen*, 2003] can be used, resulting in a modified $\hat{M}$ that is again a matrix of 1s and 0s. This is achieved by adding to the model state vector a diagnostic variable comprised of the model prediction of the measurement:

$$\hat{y}^j(t) = \left\{\psi_1 \ldots \psi_N, Q^{in}_1 \ldots Q^{in}_{N_{CEL}}, Q^{out}_1 \ldots Q^{out}_{N_{CEL}}, \hat{\theta}_1 \ldots \hat{\theta}_{N_\theta}\right\}^j, \quad j = 1, \ldots, NMC, \quad (8)$$

where N_θ is the number of measurement equivalents added to the original model state and $\hat{\theta}$ is the soil moisture computed by the model at the nodes of observation. Defining as $\hat{Y}(t_{i+1}|Z_i)$ the matrix whose columns are the NMC augmented state vectors $\hat{y}^j(t_{i+1}|Z_i)$ and as $\hat{Y}'(t_{i+1}|Z_i)$ the respective deviation from the ensemble average, equation (6) becomes:

$$y^j(t_{i+1}|Z_{i+1}) = y^j(t_{i+1}|Z_i) + \hat{K}_{i+1}\left[z^j_{i+1} - \hat{M}\hat{y}^j(t_{i+1}|Z_i)\right], \quad (9)$$

where the new Kalman gain is expressed as:

$$\hat{K}_{i+1} = Y'(t_{i+1}|Z_i)\hat{Y}'^T(t_{i+1}|Z_i)\hat{M}^T \cdot \left[\hat{M}\hat{Y}'(t_{i+1}|Z_i)\hat{Y}'^T(t_{i+1}|Z_i)\hat{M}^T + C_{\omega\omega}\right]^{-1}. \quad (10)$$

The products $Y'(t_{i+1}|Z_i)\ \hat{Y}'^T(t_{i+1}|Z_i)\hat{M}^T$ and $\hat{M}\hat{Y}'(t_{i+1}|Z_i)\hat{Y}'^T(t_{i+1}|Z_i)\hat{M}^T$ represent, respectively, the cross-covariance between the observations and all prognostic model variables and the model-predicted error covariance of the observation equivalents [*Evensen*, 2003]. Our EnKF implementation includes both options for the treatment of nonlinear M, although the first method, which involves the computation of derivatives, is not recommended due to numerical difficulties that can arise when the nonlinearity of the retention curves is strong.

[18] The computation of the covariance matrices and of the Kalman gain implemented in the CATHY model follows the square root algorithm described by *Evensen* [2004]. This algorithm allows for the use of a computationally efficient low-rank representation of the measurement error covariance matrix, thereby solving the full problem at a low cost.

[19] Finally, it should be noted that the appropriateness of the Kalman update for non-Gaussian density functions is an open issue and a potential source of suboptimality [*Reichle et al.*, 2002b].

2.3. Model Input Uncertainties and Measurement Errors

[20] In EnKF individual replicates are generated from random values of model inputs and measurement errors. It is necessary therefore to specify the probability distributions of all random variables (inputs and observations) included in our applications. The uncertain inputs selected for the test cases are saturated hydraulic conductivity K_s, porosity ϕ, residual water content θ_r, *van Genuchten* [1980] curve fitting parameters α and n, the initial pressure head at each node of the discretization grid ($\psi_i(0)$, $i = 1,\ldots, N$), and, for each simulation time step, the atmospheric forcing $u(t)$ (positive in case of rainfall, negative in case of evaporation). In order to represent uncertainty, nominal average values were set for all inputs and then perturbed by means of random fluctuations generated from a chosen PDF. In this way each realization of all the above inputs is generated and the corresponding hydrologic states are propagated over the time intervals between measurements. The resulting ensemble reflects the uncertainty introduced by input randomization.

[21] Additive normally or multiplicative lognormally distributed fluctuations were used, depending on whether the related quantity can physically assume negative values or not. Thus the ensemble of replicates for K_s, ϕ, θ_r, α, and n

Table 1. Model Discretization and Parameter Values for the Soil Column Test Case

Soil depth	100 cm
Vertical discretization (number of layers)	25
Soil layer thickness (uniform)	4 cm
Saturated hydraulic conductivity K_s	25 cm/day
Aquifer specific storage S_s	5×10^{-6} cm^{-1}
Porosity ϕ	0.54
Residual moisture content θ_r	0.20 (0.06 for scenarios D, E, F, G)
van Genuchten curve fitting parameters	$\alpha = 0.008$ cm^{-1}, $n = 1.8$ ($\alpha = 0.005$ cm^{-1}, $n = 1.7$ for scenarios D, E, F, G)
Simulation period	40 days
True initial conditions (uniform pressure head)	−50 cm
Biased initial conditions (scenarios A, B, C, D, E)	−300 cm
True atmospheric boundary conditions	−0.5 cm/day (evaporation)
Biased atmospheric boundary conditions (scenarios F, G)	−1.0 cm/day (evaporation)

were obtained by multiplying the nominal mean values ($\overline{\xi}$) by a random fluctuation:

$$\xi^j = \overline{\xi} \cdot \xi'^j, j = 1, \ldots, NMC, \tag{11}$$

where ξ^j represents the jth realization of the generic random input and ξ'^j is extracted from a lognormal distribution with unit mean and standard deviation $\sigma_{\xi'}$ chosen according to the assumed degree of uncertainty. Analogously, the perturbed initial pressure head at each node was generated by adding to the nominal mean ($\overline{\eta}$) a random fluctuation:

$$\eta^j = \overline{\eta} + \eta'^j, j = 1, \ldots, NMC, \tag{12}$$

where η'^j is extracted from a normal distribution with zero mean and standard deviation $\sigma_{\eta'}$ again chosen according to the assumed degree of uncertainty.

[22] Randomization of atmospheric forcing was carried out at each simulation time step, using equation (11) in order to preserve the positive or negative sign of the nominal values and thus avoid mistakenly switching from rainfall to evaporation or vice versa. Measurement errors were generated using equation (12) for pressure head observations and equation (11) for soil moisture and streamflow observations.

[23] In this work all random fluctuations are assumed to be spatially uncorrelated (also temporally for atmospheric forcing and observations errors). Spatial and temporal correlation structures can however be readily added, for instance to include information about soil heterogeneity.

3. Test Cases

[24] Two series of synthetic experiments were conducted. In the first the soil column experiment of *Entekhabi et al.* [1994] and *Walker et al.* [2001] was repeated to validate our data assimilation implementation by comparison with published results. Moreover, this simple test case allows the assessment of possible differences in the behavior of the filter with respect to the observation variable being assimilated (pressure head or soil moisture) within the context of a Richards equation-based simulator. In the second series a fully three-dimensional tilted v-catchment with a surface area of 1.62 km^2 is used to assess the ability of the filter to retrieve the true watershed state in terms of both subsurface and surface variables. The filter behavior is analyzed for different scenarios of assimilation data (streamflow and/or pressure head) and frequency. For both the soil column and v-catchment test cases, the open loop simulations (model runs without assimilation) and the EnKF simulations are characterized by either initial conditions or atmospheric forcing inputs that are biased with respect to the true solution.

3.1. Soil Column Experiments

[25] For these tests, forty days of synthetic soil moisture profiles (in terms of both pressure head and volumetric water content) were generated and assumed to be the true state. The soil properties, initial conditions, and boundary conditions are those of *Walker et al.* [2001] and are summarized in Table 1. *van Genuchten* [1980] moisture retention and hydraulic conductivity relationships were used. The scenarios alluded to in Table 1 refer to the 15 different configurations (Table 2) that were run in order to assess the performance of EnKF with regards to input error statistics (e.g., scenario A versus scenario B), assimilation variable (B versus C), ensemble size (e.g., D5 versus D50 versus D500), measurement error statistics (D versus E, F versus G), and simulation bias (D and E versus F and G). The filter performance is given by the root mean square error (RMSE), expressed as:

$$RMSE = \sqrt{\frac{1}{N}\sum_{i=1}^{N}\left(\frac{y_i^a - y_i^t}{y_i^t}\right)^2}, \tag{13}$$

where N is the number of grid nodes, y_i^t is the true state at the ith node, and y_i^a is the state estimate (i.e., the ensemble mean) at the ith node.

3.1.1. Comparison With Previous Work

[26] Scenario A represents the same configuration as the experiment of *Walker et al.* [2001] (here denoted as experiment W) characterized by daily updates and surface pressure head observations. Thus we can compare EnKF performance against the results obtained using an EKF retrieval algorithm in this earlier study. In this experiment the pressure head profile is initialized to a much drier condition than the true simulation (−300 cm versus −50 cm). Experiment W employs an initial state covariance matrix that in the present study corresponds to setting the coefficient of variation (CV) of the pressure head initial condition perturbations to 333% (see Table 2). For all other input errors, a CV of 5% was set, which is small enough to ensure that the filter behavior is dominated by the initial condition uncertainty, as in the work of *Walker et al.* [2001]. The CV for the measurement error was set at 1.4%, which corresponds to the 2% variance used in experiment W. All the error terms are assumed spatially uncorrelated, in order to obtain covariance matrices with large values on the

Table 2. Configurations for the Soil Column Scenarios

Scenario	Assimilated Variable (ψ or θ)	Simulation Bias (IC or BC)	Ensemble Size (NMC)	Coefficient of Variation (%) for the Model Parameters, Initial Conditions (ψ_0), Atmospheric Inputs, and Measurements				
				K_s	S_s, ϕ, θ_r, α, n	ψ_0	$u(t)$	Measured ψ or θ
A	ψ	IC	100	5	5	333	5	1.4
B	ψ	IC	100	100	5	40	50	1.4
C	θ	IC	100	100	5	40	50	1.4
D5	ψ	IC	5	100	5	20	50	1.4
D50	ψ	IC	50	100	5	20	50	1.4
D500	ψ	IC	500	100	5	20	50	1.4
E5	ψ	IC	5	100	5	20	50	84
E50	ψ	IC	50	100	5	20	50	84
E500	ψ	IC	500	100	5	20	50	84
F5	ψ	BC	5	100	5	20	50	1.4
F50	ψ	BC	50	100	5	20	50	1.4
F500	ψ	BC	500	100	5	20	50	1.4
G5	ψ	BC	5	100	5	20	50	84
G50	ψ	BC	50	100	5	20	50	84
G500	ψ	BC	500	100	5	20	50	84

diagonal and near-zero extradiagonal elements, similar to the full diagonal matrices of experiment W. The results of the simulation are shown in Figure 1, from which it can be deduced that the time needed for retrieval of the true soil moisture profile by the ensemble average (3 days, i.e., 3 updates) is the same as the one reported for the EKF scheme used by *Walker et al.* [2001]. This is also confirmed by Figure 2, which shows the behavior of RMSE versus time. After only three updates the root mean square error falls below 10%.

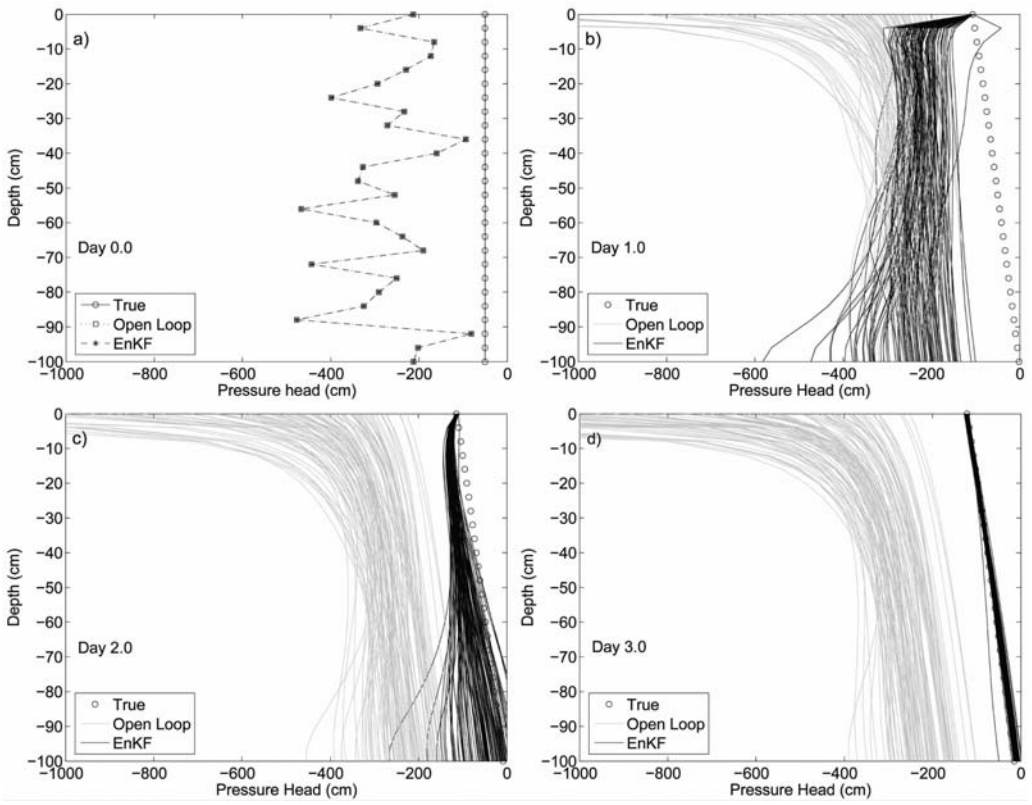

Figure 1. Pressure head profiles for the ensemble Kalman filter runs, the open loop runs, and the true solution at times (a) 0, (b) 1, (c) 2, and (d) 3 days for scenario A of the soil column test case. In Figure 1a only the average profile from the 100 starting realizations is shown. The 100 initial realizations of the open loop run are the same as those of the EnKF run.

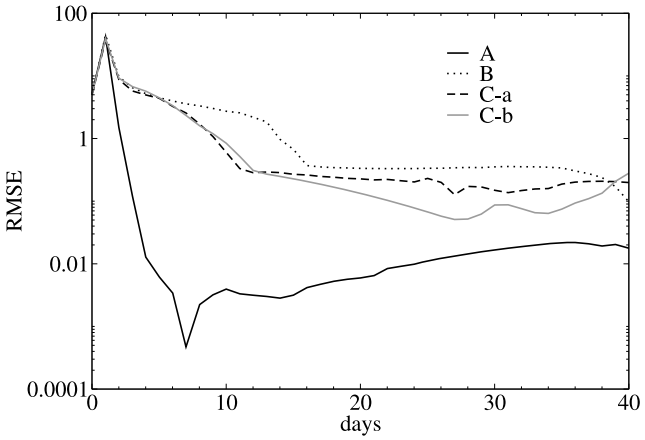

Figure 2. Time evolution of the root mean square error (RMSE) for scenarios A, B, and C of the soil column test case. C-a denotes the case in which linearization of the operator M is obtained by the state augmentation technique, while C-b denotes the case in which the numerical computation of retention curve derivatives is used.

3.1.2. Influence of Uncertainties and Measurement Operator

[27] In scenario B (as in scenario A) surface pressure head (ψ) was assimilated, whereas in scenario C the observation data represents daily surface soil moisture (θ). Assimilation of θ implies that the measurement operator M in equation (5) is nonlinear. We handled this nonlinearity using both the state augmentation technique (subscenario C-a) and the derivatives method (subscenario C-b), as was described in section 2.2.

[28] In the following experiments, the large initial condition error used in scenario A was reduced by employing a coefficient of variation equal to 40% for all other scenarios, and more importance was given to the uncertainties in saturated hydraulic conductivity and atmospheric forcing, increasing the corresponding standard deviations to 100% and 50% of the nominal mean values, respectively (see Table 2).

[29] The performance of EnKF for scenarios A, B, and C is shown in Figure 2. For the two subscenarios of C we note that there is no significant difference between the two methods used to linearize the operator M. The better performance for scenario A (faster retrieval and overall lower RMSE) is due to two effects. At first, its much larger initial condition errors relative to measurement errors cause the filter to give more weight to the measurements. As the simulation proceeds and the influence of the initial conditions wanes, the larger uncertainty on the model parameter (K_s) and error on the boundary conditions for scenarios B and C allow scenario A to maintain its better performance. The RMSE behavior for scenarios B and C is quite similar, suggesting that in this case assimilation of pressure head is as effective as assimilation of soil moisture in retrieving the true system state. It should be remarked, however, that assimilation of θ sometimes produced numerical artifacts and overshooting effects, probably linked to factors such as the treatment of nonlinear measurement operators in the state augmentation and derivatives techniques as affected by, for example, the degree of nonlinearity of the retention curves.

3.1.3. Sensitivity to Ensemble Size and Other Factors

[30] The 12 tests represented by scenarios D, E, F, and G feature (see Table 2) three ensemble sizes (5, 50, and 500), two measurement accuracies (coefficients of variation 1.4% and 84%), and two simulation biases (initial conditions and atmospheric boundary conditions; see also Table 1). Figure 3 shows that after a few days of simulation, wherein the effects of the initial conditions are dissipated, the RMSE values tend to decrease marginally, reaching an almost asymptotic behavior for scenarios D. It is also seen that the measurement error has a dominant impact on EnKF performance, with lower RMSEs attained when the observations are more reliable. On the other hand, the assimilation scheme appears to be insensitive to the ensemble size for NMC $\geq$ 50, except for a progressive smoothing of the RMSE curves as NMC increases, because of a more accurate ensemble mean evaluation.

[31] This lack of sensitivity to ensemble size may be a consequence of the one-dimensionality of the experiments and the low grid resolution. By comparison, *Evensen* [2004] found a moderate improvement in EnKF performance when increasing the ensemble size from 100 to 250 for a one-dimensional linear advection (nondissipative) model. An optimal ensemble size that balances accuracy and computational effort will depend on many factors; for the soil column experiments an ensemble size greater than 50 did not add accuracy to the data assimilation scheme.

[32] Figure 4 is analogous to Figure 3 (ensemble size and measurement error effects are represented), but here it is the surface boundary condition that is biased with respect to the true solution, rather than the initial condition. In this case lower measurement error again yields a more accurate assimilation, and higher NMC again produces smoother RMSE curves, although these effects are not as pronounced as for the biased initial condition simulations of Figure 3. In contrast to scenarios D and E, which benefit from the dissipative nature of Richards equation, the RMSEs for scenarios F and G do not progressively decrease over time. This is to be expected since the bias for these scenarios persists throughout the simulation.

3.2. V-Catchment Experiments

[33] The tilted v-catchment is made up of 50 $\times$ 81 grid cells of 20 $\times$ 20 m (Figure 5) and is characterized by an

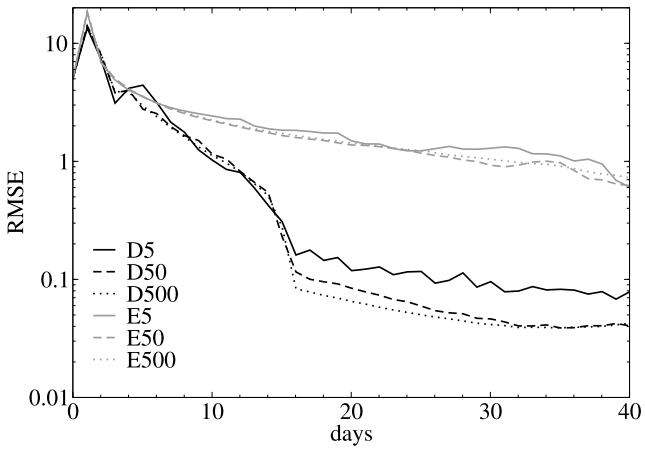

Figure 3. Time evolution of the root mean square error (RMSE) for scenarios D and E of the soil column test case.

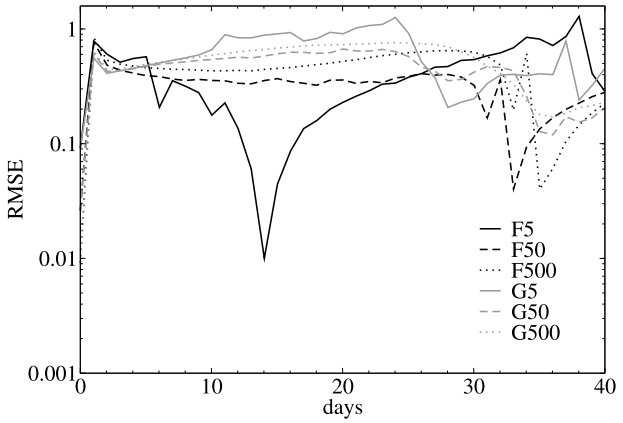

Figure 4. Time evolution of the root mean square error (RMSE) for scenarios F and G of the soil column test case.

isotropic and homogeneous aquifer of depth 3 m. Table 3 summarizes the model discretization and parameter values used for the numerical experiments. A numerical simulation was run to generate the true integration, with atmospheric boundary conditions consisting of a constant rainfall rate of 3.0×10^{-6} m/s (10.8 mm/h) from time zero to time 5400 s (1.5 h), followed by a constant evaporation rate of 3.0×10^{-7} m/s (1.08 mm/h) until the end of the simulation, at 14400 s (4 h). The initial conditions consist of a partially saturated vertical pressure head profile in hydrostatic equilibrium for the whole watershed, with a water table at 0.5 m below the surface. From the true integration, pressure head measurements at the surface and at the bottom of the catchment were extracted at 108 points evenly distributed over the catchment surface and base (so 216 pressure head observation points in total). These points are shown in Figure 5. Streamflow measurements were extracted at the catchment outlet.

[34] Twelve scenarios were run in which the following factors were varied: simulation bias (atmospheric forcing boundary conditions for scenarios 1–6; initial conditions for scenarios 7–12); assimilation variable (surface and bottom pressure head for 1, 2, 7, 8; outlet streamflow for 5, 6, 11, 12; both pressure head and streamflow for 3, 4, 9, 10); assimilation frequency (15-minute updates for 1, 3, 5, 7, 9, 11; hourly updates for 2, 4, 6, 8, 10, 12). These configurations, together with the input and measurement error statistics, are described in Table 4. For the boundary condition bias scenarios, the rainfall rate is halved with respect to the true integration and the evaporation rate is doubled. For the initial condition bias scenarios, the water table is at 1 m depth rather than 0.5 m (see Table 3). Based on the sensitivity tests conducted for the soil column experiment and on some trials carried out for the v-catchment, an ensemble size of 100 was used for all 12 scenarios. This value was found to balance accuracy and computer memory storage requirements. Open loop simulations were carried out for each scenario for comparison with the EnKF simulations. For scenarios 3, 4, 9, and 10, where both pressure head and streamflow observations were assimilated, the heads and the streamflows were normalized with the maximum values (3.0 m and 4.86 m^3/s, respectively) in order to ensure properly scaled covariance matrices [*Evensen*, 2003].

[35] The average computational time required for a single realization of all of the twelve scenarios of the v-catchment experiment is 10 minutes, indicating that the EnKF scheme is feasible for long-term (e.g., multiyear) simulations with this type of model, within the constraints of applicability of such models (generally small catchments). In terms of operational feasibility, it should also be noted that the Monte Carlo procedure that drives the EnKF algorithm is parallelizable, that the time spent by the EnKF algorithm itself is negligible compared to the CPU required for resolving the surface and subsurface schemes for each Monte Carlo realization, and that the dynamic time stepping implemented in the Richards equation solver changes (sometimes drastically) the computational time of each single realization.

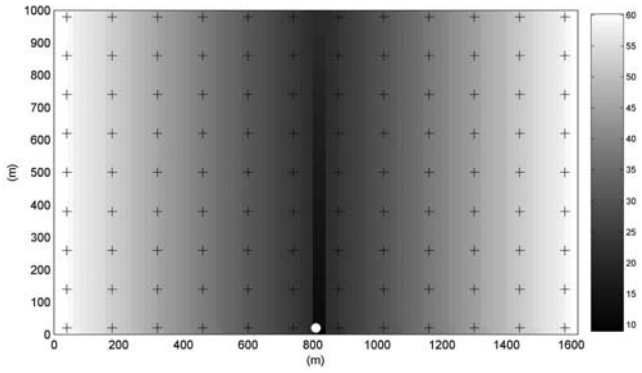

Figure 5. Digital elevation model (20 × 20 m) of the tilted v-catchment. Elevations are expressed in meters. Black crosses indicate the location of pressure head observations, and the white circle represents the location of the outlet cell, at which streamflow measurements are available.

Table 3. Model Discretization and Parameter Values for the V-Catchment Test Case

Soil depth	3 m
Vertical discretization (number of layers)	6
Soil layer thicknesses (top to bottom)	0.27, 0.36, 0.39, 0.66, 0.66, 0.66 m
Number of nodes in the three-dimensional grid	4182 × 7 = 29274
Number of tetrahedral elements in the grid	145800
Saturated hydraulic conductivity K_s	1.16×10^{-5} m/s
Aquifer specific storage S_s	5×10^{-4} m^{-1}
Porosity ϕ	0.40
Residual moisture content θ_r	0.06
van Genuchten curve fitting parameters	$\alpha = 0.47$ m^{-1}, $n = 1.70$
Simulation period	14,400 s (4.0 h)
True initial conditions (pressure head)	hydrostatic profile with water table at 0.5 m depth
Biased initial conditions (scenarios 7–12)	hydrostatic profile with water table at 1.0 m depth
True atmospheric boundary conditions	10.8 mm/h (rain) from $t = 0$ to $t = 1.5$ h, −1.08 mm/h (evaporation) from $t = 1.5$ h to $t = 4.0$ h
Biased atmospheric boundary conditions (scenarios 1–6)	5.4 mm/h (rain) from $t = 0$ to $t = 1.5$ h, −2.16 mm/h (evaporation) from $t = 1.5$ h to $t = 4.0$ h
Ensemble size NMC	100

Table 4. Configurations for the V-Catchment Scenarios

Scenario	Assimilated Variable (ψ or Q)[a]	Simulation Bias (IC or BC)	Update Interval (min)	Coefficient of Variation (%) for the Model Parameters, Initial Conditions (ψ_0), Atmospheric Inputs, and Measurements				
				K_s	S_s, ϕ θ_r, α, n	ψ_0	$u(t)$	Measured ψ or Q
1. BC-ψ-H	ψ	BC	15	100	5	20	100	1
2. BC-ψ-L	ψ	BC	60	100	5	20	100	1
3. BC-ψQ-H	ψ, Q	BC	15	100	5	20	100	1
4. BC-ψQ-L	ψ, Q	BC	60	100	5	20	100	1
5. BC-Q-H	Q	BC	15	100	5	20	100	1
6. BC-Q-L	Q	BC	60	100	5	20	100	1
7. IC-ψ-H	ψ	IC	15	100	5	40	50	1
8. IC-ψ-L	ψ	IC	60	100	5	40	50	1
9. IC-ψQ-H	ψ, Q	IC	15	100	5	40	50	1
10. IC-ψQ-L	ψ, Q	IC	60	100	5	40	50	1
11. IC-Q-H	Q	IC	15	100	5	40	50	1
12. IC-Q-L	Q	IC	60	100	5	40	50	1

[a]Pressure head ψ is measured at the soil surface and catchment base; streamflow Q is measured at the catchment outlet.

3.2.1. Scenarios With Biased Atmospheric Forcing Boundary Conditions

[36] In Figure 6 the spatial surface pressure head results between the open loop integration and the assimilation integration BC-ψ-L (scenario 2; see Table 4) are compared. Application of EnKF produces a notable reduction in model prediction error over the entire watershed surface. The improvement compared to the open loop simulation turns out to be greatest in the most unsaturated parts of the catchment, since this is where the difference between the system state and the measurements is greatest. Note that the results shown in Figure 6 are not symmetrical due to asymmetry of the subsurface grid caused by the way DEM cells are subdivided into triangles in the CATHY model [*Camporese et al.*, 2009].

[37] In Figure 7 EnKF performance is assessed in terms of its ability to improve both subsurface and surface state prediction (“a” and “b”, respectively, in the figure), under conditions where only the pressure head observations are assimilated, both head and outlet streamflow measurements are assimilated, and only streamflow is assimilated (“1”, “2”, and “3”, respectively, in the figure). In each of these 3 cases, both high frequency (15-minute, which corresponds to 1/6 of the time to peak of the streamflow hydrograph) and low frequency (hourly) EnKF results are shown, as well as the open loop and true solutions. From the results shown in Figure 7 it can be concluded that assimilation of pressure head alone at low frequency is not sufficient to retrieve the catchment response in terms of streamflow, whereas a slight improvement with respect to the open loop run is achieved with high frequency assimilation. The results improve with the integrated assimilation of all the measurements, but the best response in terms of outlet streamflow, for both update intervals, is produced by assimilation of streamflow only. Although it appears, from “2b” and “3b” in Figure 7, that low frequency assimilation performs better than the runs with frequent updates in terms of outlet streamflow, on closer inspection it can be seen that, for scenario BC-Q-L, only the hydrograph peak is better matched, whereas the high frequency run (BC-Q-H) matches the time to peak and total streamflow volume better (14861 m^3 for BC-Q-L and 15714 m^3 for BC-Q-H, versus 19684 m^3 for the true simulation). On the other hand, the comparison between scenarios BC-ψQ-L and BC-ψQ-H results indeed in a better outlet streamflow retrieval for the low frequency run. Nonetheless, the true subsurface state is better captured by the high frequency run.

[38] The improvement in the retrieval of the outlet hydrograph when assimilating streamflow measurements comes at the expense of a poorer retrieval of the catchment response in terms of subsurface state. Comparison of “1a”, “2a”, and “3a” in Figure 7 shows that satisfactory retrieval of the subsurface storage volumes is attained only when pressure head is assimilated. Assimilation of streamflow alone causes an instantaneous increase in the surface discharge, followed by a reduction in the water content in the catchment. This seems to provide the water needed to sustain surface runoff. Indeed, at the end of the BC-Q-H and BC-Q-L integrations, subsurface water storage is even less than for the open loop simulations, with a difference between these runs that is of the same order of magnitude as the difference between the surface hydrographs. Note that these compensatory differences are on the order of 10^3 m^3, compared to a total subsurface storage volume of order 10^6 m^3. Thus it may be argued that low frequency assimilation of pressure head and/or volumetric water content should be carried out during moderate flow regimes, while high frequency assimilation of discharge is useful during short-term flood events to accurately reproduce the hydrograph. After the flood event, the model is in a state analogous to that of a biased initial condition scenario, so the assimilation can switch back to low frequency subsurface updates to retrieve the true aquifer water content and, consequently, to reduce prediction errors for subsequent flood events.

[39] Overall, for these scenarios with biased surface boundary conditions, it is found, as expected, that the dynamics is controlled by the atmospheric forcing. In fact, after each update the system will tend to the same state as the open loop simulation, since the ensemble Kalman filter, as implemented in this application, does not have the capability to maintain an update over a protracted time period.

3.2.2. Scenarios With Biased Initial Conditions

[40] Figure 8 is analogous to Figure 7 but presents the results of the scenarios with biased initial conditions (scenarios 7–12 of Table 4). These results are broadly consis-

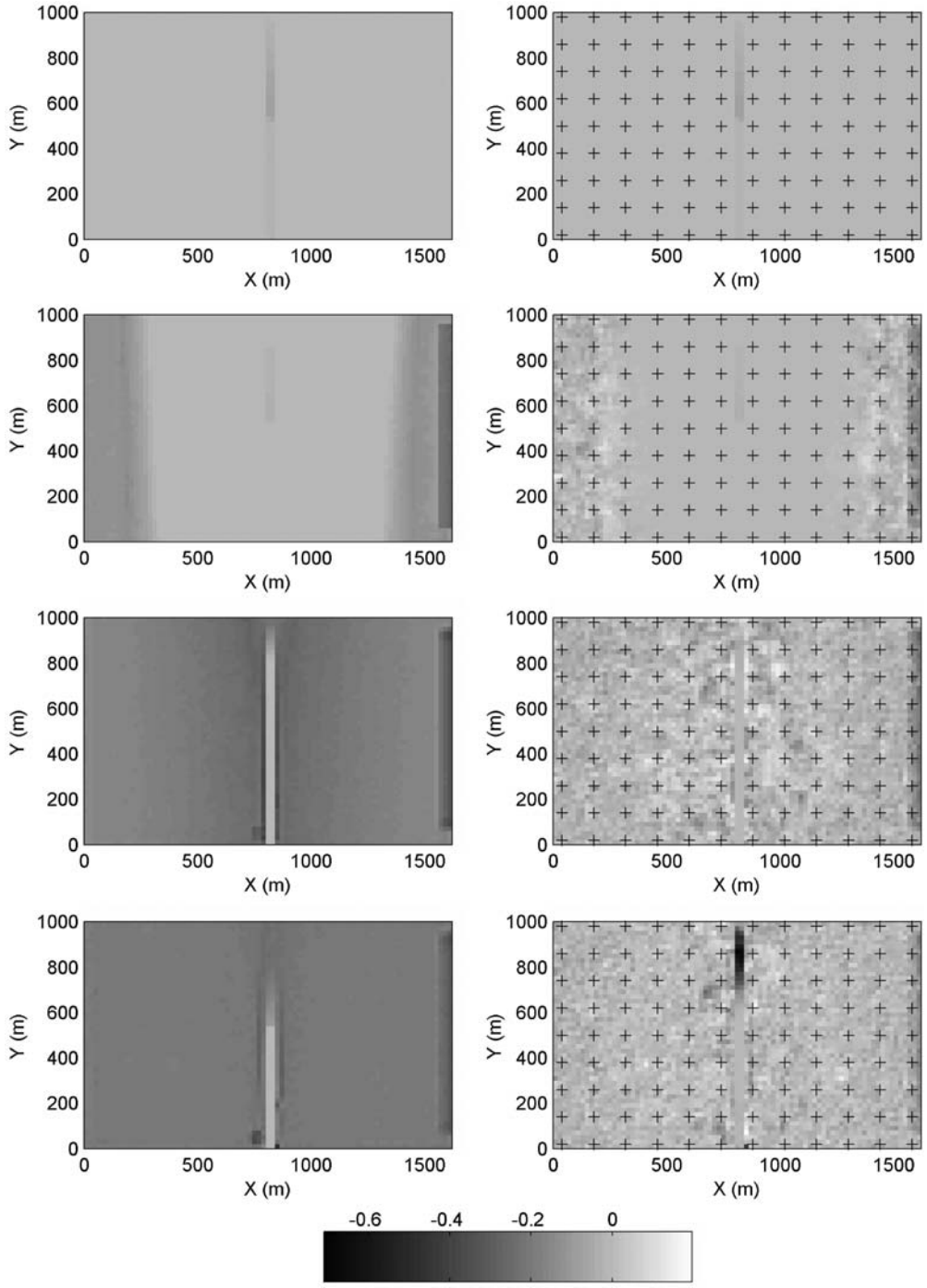

Figure 6. Differences (m) at the surface (left) between the true pressure head and the open loop ensemble mean pressure head and (right) between the true pressure head and the scenario 2 (BC-ψ-L) ensemble mean pressure head at times 1, 2, 3, and 4 h (from top to bottom). Black crosses show the location of the hourly observations.

tent with those reported in Figure 7 for the biased boundary condition scenarios, with a few notable differences. In these scenarios assimilation of pressure head alone improves significantly the streamflow prediction, even though it is not sufficient for a complete retrieval. The best outlet streamflow retrieval, together with the subsurface volume retrieval, is obtained for scenario 9, when all observation data is assimilated at high frequency. High frequency assimilation of streamflow data alone (scenario 11) is not only unable to retrieve the true hydrograph, but it also produces numerical artifacts in surface pressure heads, with some nodes yielding unrealistic (and nonphysical) values. This behavior with respect to the subsurface state is likely due to the loss of information introduced by the projection of the covariance matrix onto the measurement space, which in this case has the dimension of a scalar, i.e., rank one. The resulting covariance matrix between the streamflow at the outlet and the pressure head system state is in fact a vector

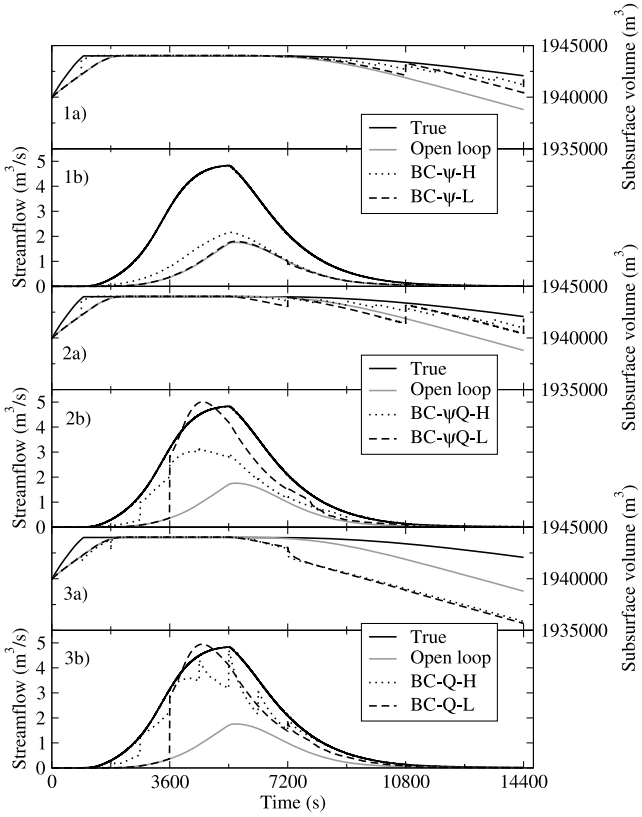

Figure 7. Subsurface water storage and outlet hydrograph for the true solution, the ensemble mean of the open loop integrations, and the ensemble mean of the assimilation integrations for the v-catchment test case. The assimilation runs correspond to scenarios 1–6 of Table 4 (biased atmospheric boundary conditions), with the same bias applied to the open loop run.

with values that show a quasirandom behavior, as we will see below. This reflects the aggregated nature of streamflow observed at the outlet of a catchment: it is an integral measure of overland flow occurring on the entire watershed, and as such it is not able to drive the DA algorithm toward a satisfactory description of the distributed nature of runoff generation and, by extension, of the subsurface state responsible for this generation. This results in extreme underestimation of subsurface water storage. On examination of Figure 8, what appears to occur for scenario 11 (IC-Q-H) is that after each update there is a mass exchange from the surface toward the subsurface, corresponding to a decrease in streamflow and a related increase in the groundwater volume. Intuitively, during streamflow assimilation, the DA algorithm tends to add water mainly to the surface because this is the domain being assimilated and because of the lower variability inherent in the saturated zone. The dynamics of the system subsequently redistributes this mass into the subsurface because the soil is not completely saturated. Since in this case it is the saturated groundwater flow dynamics that acts as streamflow generation mechanism (Dunne runoff), in the absence of compensatory information about the internal state of the catchment/aquifer (e.g., pressure head measurements), and in response to successive streamflow-based updates, the subsurface solution progressively and dramatically diverges from the true solution.

[41] The above considerations do not explain the large variations of the subsurface volume observed in correspondence of the updates (Figure 8, 3a). To further investigate the behavior of the EnKF algorithm when assimilating streamflow only, we carried out another series of simulations for scenarios 11 and 12 to test for ill-conditioning of the Kalman gain, in particular with regards to the covariance matrix between outlet streamflow and distributed pressure heads. For scenario 11 we changed the seed used to initialize the random generator. For scenario 12, in addition, we increased the ensemble size. Figure 9 shows the impact of the choice of initial seed (1 and 2) and the ensemble size (3). The true and the open loop runs are the same as in Figure 8 and are not shown here. The results confirm our hypothesis. While for the first value of initial seed the results in 1a and 1b are consistent with those reported in Figure 8 (3), the second value of initial seed produces a very different behavior both for the subsurface volume and the streamflow (Figure 9, 2a and 2b). The first update in particular shows an akward behavior: in the deeper soil layers the algorithm removes water, while it increases the pressure head only at the surface. The outcome is that the subsurface storage is globally reduced and the surface has

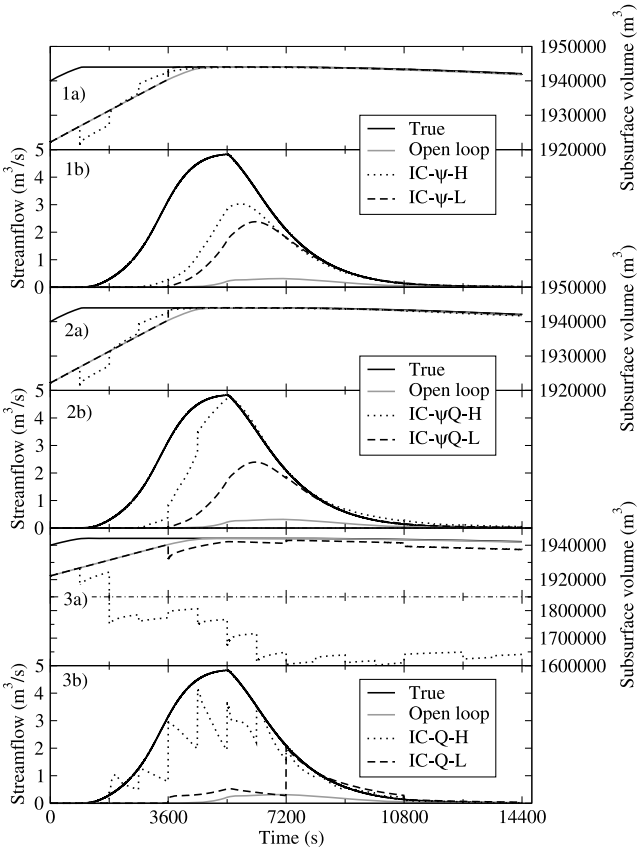

Figure 8. Subsurface water storage and outlet hydrograph for the true solution, the ensemble mean of the open loop integrations, and the ensemble mean of the assimilation integrations for the v-catchment test case. The assimilation runs correspond to scenarios 7–12 of Table 4 (biased initial conditions), with the same bias applied to the open loop run.

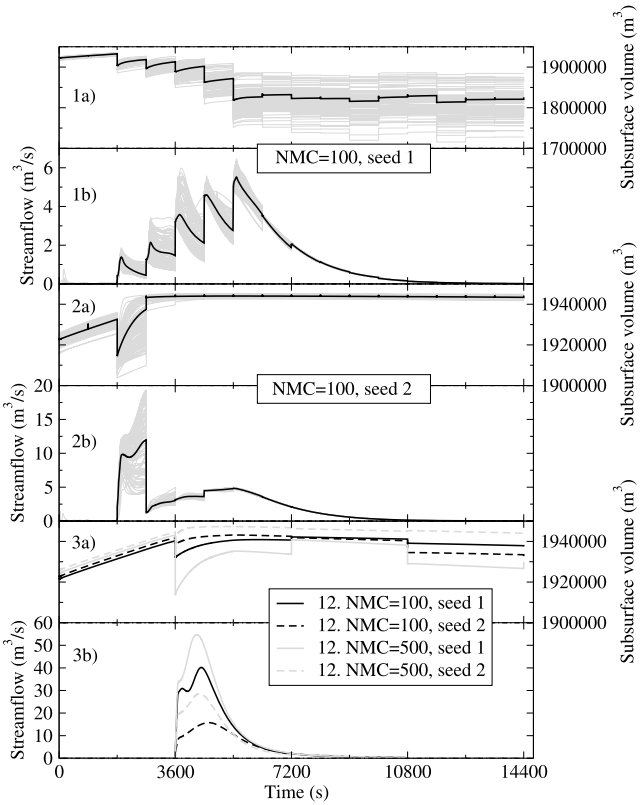

Figure 9. Subsurface water storage and outlet hydrograph for the assimilation integrations of the v-catchment test case. The assimilation runs correspond to scenarios 11 and 12 of Table 4 (biased initial conditions) and show the effect of changing the seed used to initialize the random generator (1 and 2) and the ensemble size (3). In 1 and 2 the light gray lines represent the ensemble of realizations, while the thick black lines correspond to the ensemble means.

an excess of water to be routed to the outlet, as demonstrated by the overestimated peak right after the update. Later updates have little impact on the subsurface due to the fact that the watershed becomes almost completely saturated, and, as such, uncorrelated with the streamflow at the outlet. As a consequence, the streamflow recovers the true pattern. Similar conclusions can be drawn for the low frequency scenario 12 (Figure 9, 3). Here the subsurface volume is not dramatically underestimated, as the first update is performed at t = 3600 s, i.e., when the watershed is almost saturated. Note that increasing the ensemble size does not produce any benefit for the assimilation, confirming that the covariance matrix between streamflow and pressure head is responsible for this odd behavior.

4. Conclusions

[42] The ensemble Kalman filter has been implemented and evaluated for a coupled catchment scale hydrological model of surface and subsurface flow. The advantages of the EnKF data assimilation scheme for this distributed process-based model include: ease of implementation; consideration of model nonlinearities without costly Jacobian calculations; ability to account for different sources of uncertainty (soil parameters, atmospheric forcing, initial conditions); and the possibility to assimilate concurrent observation data sets, both gridded and scattered, from different measurement sources. The disadvantages relate to the need to construct, store, and manipulate large covariance matrices and the computational effort required when a large ensemble size is combined with a large model grid. An important aspect that needs to be carefully studied concerns the appropriateness of the Kalman update for non-Gaussian density functions.

[43] The numerical experiments conducted show that EnKF is successful in decreasing the error between simulated and observed values for both one- and three-dimensional test cases. A sensitivity analysis carried out to assess the impact of ensemble size on the filter performance showed that, at least for the one-dimensional test case presented here, the scheme is robust and that a relatively limited number of realizations ($\sim$50) is sufficient for a satisfactory level of accuracy in state variable retrieval. For the soil column experiments, EnKF was effective independently of the variable being assimilated, even though assimilation of moisture content in a pressure head-based subsurface solver raises some numerical issues linked to the handling of nonlinear measurement operators and to the degree of nonlinearity of the retention curves. Reliable observations improved the filter's performance significantly, but this result depended also on the relative level of confidence given to the model inputs.

[44] For the v-catchment experiments the situation is more complicated because the system state is composed of both subsurface and surface variables. In this case it was important to measure the state variable of interest. For instance while assimilation of pressure head alone generally improved the system state in terms of both subsurface and surface variables, assimilation of streamflow data alone did not improve the subsurface state, and indeed even worsened it with respect to the open loop integrations, due to the ill-conditioned covariance matrix between streamflow at the outlet and node-based distributed pressure heads. This implies that assimilation of streamflow alone during one storm may lead to incorrect simulations for the next storm if the initial groundwater volume is misestimated. The best retrieval of the overall catchment state (surface and subsurface systems) was achieved by joint assimilation of pressure head and streamflow. A higher assimilation frequency (relative to the time to peak of the streamflow) improved the retrieval of the system state globally only in the case of joint assimilation. When streamflow (pressure head) was assimilated alone, the benefits of more frequent updates were limited to the surface (subsurface) system state.

[45] In the case of streamflow assimilation it is possible to improve performance by implementing a smoother, or retrospective filtering approach [e.g., *Pauwels and De Lannoy*, 2006], i.e., updating the state of the catchment not only at the current time step but also at a number of previous time steps. This option is worthy of further investigation and raises some interesting issues for a detailed coupled model, for instance determining the optimal size of the backward assimilation window, and dealing with the computational challenges arising from such backward assimilation.

[46] Other possible topics for future work on data assimilation for physically based catchment models include:

comparing EnKF to the more efficient (in CPU and memory) but less optimal nudging scheme, previously implemented in the CATHY model; improving EnKF's propagation of updates in time, for better performance in particular when atmospheric forcing is biased; and implementing more advanced randomization of soil properties to take into account spatial correlation structures (e.g., spatial variability of hydraulic conductivity).

[47] **Acknowledgments.** We acknowledge the financial support of the Ouranos Consortium and the Natural Sciences and Engineering Research Council of Canada (project CRDPJ-319968-04), the University of Padova (research fellowship CPDR075551/07), and the Italian Ministry of Education, University, and Scientific Research (PRIN 2007 projects 200788W4EC and 20074TZWNJ). We thank the editors and two anonymous reviewers for their detailed and very helpful comments.

References

Aubert, D., C. Loumagne, and L. Oudin (2003), Sequential assimilation of soil moisture and streamflow data in a conceptual rainfall-runoff model, *J. Hydrol.*, *280*, 145–161.

Bixio, A. C., S. Orlandini, C. Paniconi, and M. Putti (2000), Physically-based distributed model for coupled surface runoff and subsurface flow simulation at the catchment scale, in *Computational Methods in Water Resources*, vol. 2, *Computational Methods, Surface Water Systems and Hydrology*, edited by L. R. Bentley et al., pp. 1115–1122, Balkema, Rotterdam, Netherlands.

Camporese, M., C. Paniconi, M. Putti, and S. Orlandini (2009), Surface-subsurface flow modeling with path-based runoff routing, boundary condition-based coupling, and assimilation of multisource observation data, *Water Resour. Res.*, doi:10.1029/2008WR007536, in press.

Chen, Y., and D. Zhang (2006), Data assimilation for transient flow in geologic formations via ensemble Kalman filter, *Adv. Water Resour.*, *29*, 1107–1122.

Chen, F., K. Mitchell, J. Schaake, Y. Xue, H. L. Pan, V. Koren, Q. Y. Duan, M. Ek, and A. Betts (1996), Modeling of land-surface evaporation by four schemes and comparison with FIFE observations, *J. Geophys. Res.*, *101*(D3), 7251–7268.

Clark, M. P., D. E. Woods, R. A. Woods, X. Zheng, R. P. Ibbitt, A. G. Slater, J. Schmidt, and M. J. Uddstrom (2008), Hydrological data assimilation with the ensemble Kalman filter: Use of streamflow observations to update states in a distributed hydrological model, *Adv. Water Resour.*, *31*, 1309–1324.

Crow, W. T., and E. Van Loon (2006), Impact of incorrect model error assumptions on the sequential assimilation of remotely sensed surface soil moisture, *J. Hydrometeorol.*, *7*(3), 421–432.

Dai, Y., et al. (2003), The common land model (CLM), *Bull. Am. Meteorol. Soc.*, *84*, 1013–1023.

Das, N. N., and B. P. Mohanty (2006), Root zone soil moisture assessment using remote sensing and vadose zone modeling, *Vadose Zone J.*, *5*, 296–307.

De Lannoy, G. J. M., R. H. Reichle, P. R. Houser, V. R. N. Pauwels, and N. E. C. Verhoest (2007), Correcting for forecast bias in soil moisture assimilation with the ensemble Kalman filter, *Water Resour. Res.*, *43*, W09410, doi:10.1029/2006WR005449.

Drécourt, J.-P., H. Madsen, and D. Rosbjerg (2006), Calibration framework for a Kalman filter applied to a groundwater model, *Adv. Water Resour.*, *29*, 719–734.

Entekhabi, D., H. Nakamura, and E. G. Njoku (1994), Solving the inverse problem for soil moisture and temperature profiles by sequential assimilation of multifrequency remotely sensed observations, *IEEE Trans. Geosci. Remote Sens.*, *32*(2), 438–448.

Evensen, G. (1994), Sequential data assimilation with a nonlinear quasi-geostrophic model using Monte Carlo methods to forecast error statistics, *J. Geophys. Res.*, *99*(C5), 10,143–10,162.

Evensen, G. (2003), The ensemble Kalman filter: Theoretical formulation and practical implementation, *Ocean Dyn.*, *53*, 343–367.

Evensen, G. (2004), Sampling strategies and square root analysis schemes for the EnKF, *Ocean Dyn.*, *54*, 539–560.

Hantush, M. M., and M. A. Mariño (1997), Estimation of spatially variable aquifer hydraulic properties using Kalman filtering, *J. Hydraul. Eng. ASCE*, *123*(11), 1027–1035.

Hoeben, R., and P. A. Troch (2000), Assimilation of active microwave observation data for soil moisture profile estimation, *Water Resour. Res.*, *36*(10), 2805–2819.

Kalman, R. E. (1960), A new approach to linear filtering and prediction problems, *J. Basic Eng.*, *82*, 35–45.

Kollet, S. J., and R. M. Maxwell (2006), Integrated surface-groundwater flow modeling: A free-surface overland flow boundary condition in a parallel groundwater flow model, *Adv. Water Resour.*, *29*(7), 945–958.

Kollet, S. J., and R. M. Maxwell (2008a), Capturing the influence of groundwater dynamics on land surface processes using an integrated, distributed watershed model, *Water Resour. Res.*, *44*, W02402, doi:10.1029/2007WR006004.

Kollet, S. J., and R. M. Maxwell (2008b), Demonstrating fractal scaling of baseflow residence time distributions using a fully-coupled groundwater and land surface model, *Geophys. Res. Lett.*, *35*, L07402, doi:10.1029/2008GL033215.

Koster, R., and M. Suarez (1996), Energy and water balance calculation in the mosaic LSM, *Tech. Memo. 1046069*, NASA GSFC, Greenbelt, Md.

Kosugi, K., S. Katsura, T. Mizuyama, S. Okunaka, and T. Mizutani (2008), Anomalous behavior of soil mantle groundwater demonstrates the major effects of bedrock groundwater on surface hydrological processes, *Water Resour. Res.*, *44*, W01407, doi:10.1029/2006WR005859.

Liang, X., E. F. Wood, and D. P. Lettenmaier (1996), Surface soil moisture parameterization of the VIC-2L model: Evaluation and modifications, *Global Planet. Change*, *13*, 195–206.

Mackay, D. S., and L. E. Band (1998), Extraction and representation of nested catchment areas from digital elevation models in lake-dominated topography, *Water Resour. Res.*, *34*(4), 897–901.

Margulis, S. A., D. McLaughlin, D. Entekhabi, and S. Dunne (2002), Land data assimilation and estimation of soil moisture using measurements from the Southern Great Plains 1997 Field Experiment, *Water Resour. Res.*, *38*(12), 1299, doi:10.1029/2001WR001114.

Maxwell, R. M., and S. J. Kollet (2008), Interdependence of groundwater dynamics and land-energy feedbacks under climate change, *Nat. Geosci.*, *1*, 665–669.

McLaughlin, D. (2002), An integrated approach to hydrologic data assimilation: Interpolation, smoothing, and filtering, *Adv. Water Resour.*, *25*, 1275–1286.

Miller, R. N., M. Ghil, and F. Gauthiez (1994), Advanced data assimilation in strongly nonlinear dynamical systems, *J. Atmos. Sci.*, *51*, 1037–1056.

Montgomery, D. R., and E. Foufoula-Georgiou (1993), Channel network source representation using digital elevation models, *Water Resour. Res.*, *29*(12), 3925–3934.

Morita, M., and B. C. Yen (2002), Modeling of conjunctive two-dimensional surface-three-dimensional subsurface flows, *J. Hydraul. Eng. ASCE*, *128*(2), 184–200, doi:10.1061/(ASCE)0733-9429(2002)128:2(184).

Orlandini, S., and R. Rosso (1996), Diffusion wave modeling of distributed catchment dynamics, *J. Hydraul. Eng. ASCE*, *1*(3), 103–113.

Panday, S., and P. S. Huyakorn (2004), A fully coupled physically-based spatially-distributed model for evaluating surface/subsurface flow, *Adv. Water Resour.*, *27*, 361–382, doi:10.1016/j.advwatres.2004.02.016.

Paniconi, C., and M. Putti (1994), A comparison of Picard and Newton iteration in the numerical solution of multidimensional variably saturated flow problems, *Water Resour. Res.*, *30*(12), 3357–3374.

Paniconi, C., M. Marrocu, M. Putti, and M. Verbunt (2003), Newtonian nudging for a Richards equation-based distributed hydrological model, *Adv. Water Resour.*, *26*, 161–178.

Pauwels, V. R. N., and G. J. M. De Lannoy (2006), Improvement of modeled soil wetness conditions and turbulent fluxes through the assimilation of observed discharge, *J. Hydrometeorol.*, *7*(3), 458–477.

Putti, M., and C. Paniconi (2004), Time step and stability control for a coupled model of surface and subsurface flow, in *Proceedings of the XV International Conference on Computational Methods in Water Resources (CMWR XV)*, vol. 2, pp. 1391–1402, Elsevier, New York.

Reichle, R. H., and R. D. Koster (2003), Assessing the impact of horizontal error correlations in background fields on soil moisture estimation, *J. Hydrometeorol.*, *4*(6), 1229–1242.

Reichle, R. H., J. P. Walker, R. D. Koster, and P. R. Houser (2002a), Extended versus ensemble Kalman filtering for land data assimilation, *J. Hydrometeorol.*, *3*(6), 720–728.

Reichle, R. H., D. B. McLaughlin, and D. Entekhabi (2002b), Hydrologic data assimilation with the ensemble Kalman filter, *Mon. Weather Rev.*, *130*, 103–114.

Van Geer, F. C., C. B. M. Te Stroet, and Z. Yangxiao (1991), Using Kalman filtering to improve and quantify the uncertainty of numerical groundwater simulations: 1. The role of system noise and its calibration, *Water Resour. Res.*, *27*(8), 1987–1994.

van Genuchten, M. T. (1980), A closed-form equation for predicting the hydraulic conductivity of unsaturated soils, *Soil Sci. Soc. Am. J.*, *44*, 892–898.

VanderKwaak, J. E., and E. A. Sudicky (1999), Application of a physically-based numerical model of surface and subsurface water flow and solute transport, in *ModelCARE 99 Proceedings of the International Conference on Calibration and Reliability in Groundwater Modeling: Coping with Uncertainty*, edited by F. Stauffer et al., pp. 641–648, ETH Zurich, Zurich, Switzerland.

Walker, J. P., and P. R. Houser (2001), A methodology for initializing soil moisture in a global climate model: Assimilation of near-surface soil moisture observations, *J. Geophys. Res.*, *106*(D11), 11,761–11,774.

Walker, J. P., G. R. Willgoose, and J. D. Kalma (2001), One-dimensional soil moisture profile retrieval by assimilation of near-surface observations: A comparison of retrieval algorithms, *Adv. Water Resour.*, *24*, 631–650.

Wörman, A., A. I. Packman, L. Marklund, J. W. Harvey, and S. H. Stone (2007), Fractal topography and subsurface water flows from fluvial bedforms to the continental shield, *Geophys. Res. Lett.*, *34*, L07402, doi:10.1029/2007GL029426.

M. Camporese and P. Salandin, Dipartimento di Ingegneria Idraulica, Marittima, Ambientale e Geotecnica, Università degli Studi di Padova, via Loredan 20, I-35131 Padova, Italy. (camporese@idra.unipd.it; sala@idra.unipd.it)

C. Paniconi, Institut National de la Recherche Scientifique, Centre Eau, Terre et Environnement, Université du Québec, 490 de la Couronne, Québec, QC G1K 9A9, Canada. (claudio.paniconi@ete.inrs.ca)

M. Putti, Dipartimento di Metodi e Modelli Matematici per le Scienze Applicate, Università degli Studi di Padova, via Trieste 63, I-35121 Padova, Italy. (putti@dmsa.unipd.it)